CdSe Core–Shell Nanoparticles as Active Materials for Up-Converted Emission

ARTICLE *in* THE JOURNAL OF PHYSICAL CHEMISTRY C · FEBRUARY 2011

Impact Factor: 4.77 · DOI: 10.1021/jp107489t

THE JOURNAL OF PHYSICAL CHEMISTRY C

ARTICLE

pubs.acs.org/JPCC

CdSe Core−Shell Nanoparticles as Active Materials for Up-Converted Emission

Ilaria Fortunati,[†] Raffaella Signorini,[†,*] Renato Bozio,[†] Jacek. J. Jasieniak,[‡] Alessandro Antonello,[§] Alessandro Martucci,[§] Gioia Della Giustina,[§] Giovanna Brusatin,[§] and Massimo Guglielmi[§]

[†]Department of Chemical Science and INSTM Research Unit, University of Padova, Via Marzolo 1, 35131, Padova, Italy

[‡]CSIRO, Materials Science and Engineering, Ian Wark Laboratory, Bayview Avenue, Clayton 3168, Australia

[§]Department of Mech. Eng.-Materials Section, University of Padova

ABSTRACT: In this study, we investigate CdSe based core−shell quantum dots as potential active materials for nonlinear optical applications. A detailed characterization of the linear and nonlinear optical properties is carried out for QDs in solution and within two electronically similar sol−gel hosts, hafnia and zirconia. The favorable absorption and emission properties of the solid-state hybrid sol−gel/QD matrices are exploited for the realization of up cavity-less laser.

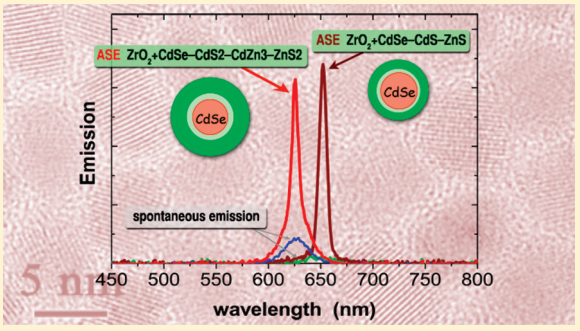

1. INTRODUCTION

Solid-state active materials, emitting in the infrared region of the spectrum, are heavily used in current laser technologies, finding application in telecommunication and for investigating ultrafast processes in a wide variety of physics-, chemistry-, and biology-related problems.[1,2] The extension of IR wavelengths toward the visible region of the electromagnetic spectrum also has significant use, advancing areas where lasing with shorter wavelength and/or visible colors are required, optical recording and image processing being two examples.[3−5] To this extent, the process of creating visible wavelength laser light can be realized directly through the fabrication of semiconductor diodes, such as those based on alloys with GaN[6] or through the up-conversion of IR sources: a process where light is emitted with photon energies higher than those of the light generating the excitation.[7]

Up-converted light emission can be achieved directly through optical pumping of a material at energies smaller than its optical gap, provided that the material possesses a large nonlinear absorption coefficient and efficient fluorescence emission. Through a two-photon absorption (TPA) process, a simultaneous absorption of two photons, a chromophore is excited from the ground to the excited state. Fluorescence occurs from the one-photon allowed state that is populated by relaxation from the initially excited two-photon state. Overall, this process permits the emission wavelength to be shorter than that of the laser pump.[8] The major advantages of up-conversion through TPA are: i) elimination of phase-matching requirements necessary for harmonic generation, ii) the feasibility of using IR lasers as pump sources, and iii) the capability of adopting film, waveguide, and fiber configurations. However, a continuing challenge that must be addressed to fully harness these advantages within real-world technologies remains the development of chromophores with high nonlinear coefficients and fluorescence quantum yields. To date, a wide variety of chromophores with large two-photon activities have been already reported, spanning from organic small molecules[9,10] to polymers[11] and inorganic semiconductors.[12] Among these, inorganic quantum dots (QDs) have exhibited some of the highest two-photon absorption cross sections (σ_{TPA}), reaching values of 50 000 GM.[13] This factor has permitted such materials to be used for up-converted optical gain applications, including highly efficient amplified spontaneous emission (ASE) and lasing.[14,15]

QDs are low-dimensional nanoscale materials that exhibit size-dependent optical and physical properties.[16] For many strongly confined QDs, the spacing between the lowest electronic states is much greater than the available thermal energy. This inhibits thermal depopulation of the lowest electronic state, which allows for them to be sequentially filled with electrons and holes. The process of state filling is at the heart of many phenomena that is observed for QDs, including optical gain and quantized conductivity.[17,18] It is also fundamentally related to QDs exhibiting high yielding photoluminescence, which can be continuously varied over a wide energy range by merely changing the particle size. This versatility makes QDs a promising candidate for the realization of devices based on their optical and electrical properties.[19−21] For instance, they have been successfully employed as biolabels for In Vivo and in vitro studies,[22,23] in the

Received: August 9, 2010
Revised: January 27, 2011
Published: February 23, 2011

development of screening techniques using multiplexing technologies,[24] and as fluorophores in fluorescence lifetime imaging.[25] They have also been tested as active materials for the realization of innovative technological devices, like LEDs[26] and lasers.[27−29]

We have recently demonstrated the viability of using the up-conversion properties of QDs to generate optical gain capable of being exploited for amplified spontaneous emission (ASE) in a 1D slab waveguide configuration.[14] Here, we extend that work by studying the multiphotonic absorption properties of a variety of commercial and in-house synthesized CdSe-based core−shell QDs, both in solution and as dopants within sol−gel hybrid matrices. Such sol−gel matrices have been found to be vital for ensuring high photophysical stability of QDs under conditions necessary to achieve optical gain. To further understand the electronic requirements of QD host materials that will permit stable optical gain, in this work we compare two electronically similar sol−gel matrices, zirconia and hafnia, as hosts. The similarity in their electronic structure suggests that within these matrices, identical QDs should exhibit comparable photophysical behaviors.[30] This hypothesis, which is necessary to establish a general material criteria for developing appropriate QD hosts, is tested by comparing the optical features of QD/sol−gel hybrids, based on both host materials, directly under up-converted ASE conditions.

2. EXPERIMENTAL METHODS

2.1. Commercial CdSe-Based Core−Shell Samples. The EviDot core−shell nanocrystal samples were purchased from Evident Technologies. As specified on the certification sheets, the toluene dispersed nanocrystals possessed diameters of 4.6 and 5.5 nm, and are commercially termed "Birch-Yellow" and "Maple Red-Orange", respectively.

2.2. Synthesis of In-House CdSe-Based Core−Shell Samples. The in-house made CdSe based core−shell nanocrystals were synthesized according to established salt-based methods in 1-octadecene.[12,31,32] Two different core−shell structures were synthesized and studied: (i) "CdSe−CdS2−$Cd_{0.5}Zn_{0.5}$S3−ZnS2" nanocrystals (hereafter called "CdSe−CdS2−CdZn3−ZnS2") possessing a graded seal shell with seven monolayers in total, starting from a 3.5 nm diameter core, and (ii) "CdSe−CdS1−$Cd_{0.5}Zn_{0.5}$S1−ZnS1" (hereafter called "CdSe−CdS−ZnS") with an external shell of three graded seal monolayers, with a 5.3 nm diameter core.

In a typical core−shell synthesis, 1 μmol of CdSe nanocrystals were dispersed in a 1:1 by weight mixture of octadecylamine and 1-octadecene to give a nanocrystal concentration of 40 μM. This solution was heated to 60 °C under nitrogen and pump purged three times. The CdSe nanocrystals were then heated at a temperature ranging between 200 and 225 °C (depending on the size of the nanoparticle) under nitrogen for the injection of the first layer enriched of $Cd(TMPPA)_2$, where TMPPA is the bis-(2,2,4-trimethylpentyl)phosphinic acid. For the growth of the metal and chalcogenide layers, we used a 0.1 M solution of cadmium oxide or zinc acetate dianhydride dissolved by an 8-fold molar excess of TMPPA in ODE and sulfur dissolved in ODE, respectively.[31] The appropriate quantity of monomer calculated, based on a concentric shell model, was then added layer-by-layer. To avoid homogeneous nucleation, a 1:2 molar ratio of triphenyl phosphine:sulfur was injected prior to each S addition. Metal and chalcogenide layers were allowed to grow for 15 min each, with the temperature being increased by 10 °C with every semiconductor ML up to a maximum of 245 °C. A 20% excess of the metal layers was used to ensure high PL and high photostability of the resulting particles.[34] The resulting QDs were purified through multiple extractions using chloroform/methanol/acetone mixtures.

2.3. Preparation of QD-Doped Solid Samples Based on Sol−Gel Host Matrices. The synthesis of the zirconia (ZrO_2) matrix was based on that previous data reported in ref 14. The hafnia (HfO_2)-based hybrid was prepared in a similar manner, using Hf-butoxide as a precursor instead of Zr-isopropoxide. Both Zr and Hf sol-solutions are stirred for one hour before being filtered through a 0.20 μm PTFE filter and then mixed with quantum dots dispersed in isopropanol. The QD/sol solution is spin coated on quartz slides at 3500 rpm for 20 s under Ar atmosphere to prevent degradation. The film was treated at 100 °C for 2 min and at 250 °C for 5 min.

2.4. Optical Characterization. The linear absorption and emission spectra were recorded with a Cary 5 spectrophotometer and a FluoroMax-P (Jobin−Yvon) fluorimeter. Fluorescence quantum yields (FQY) of the commercial and in-house QDs were respectively determined by calibration against Rhodamine B (FQ = 0.8) or Cresyl Violet (FQY = 0.66) standards in methanol.[35−37]

The nonlinear optical characterization of the QDs in solution was performed employing a Ti-sapphire laser system (Coherent, mod. Mira Optima 900-F). It delivers pulses with duration time of ∼150 fs, in the wavelength range from 700 to 1000 nm, with a 76 MHz repetition rate and ∼10 nJ pulse energy at 800 nm.

The ultrafast laser pulses were used to measure the two photon absorption cross section in solutions through the two-photon induced fluorescence (TPIF) technique, following the method described in ref 38. The incident beam was focused through a 40 cm lens onto a 10 mm cuvette containing the sample solution. The TPA cross-section was determined using the formula:

$$\sigma^{S}_{TPA} = \sigma^{R}_{TPA}\frac{\langle F\rangle_S}{\langle F\rangle_R}\frac{C_R}{C_S}\frac{\eta_R}{\eta_S}\frac{\phi_R}{\phi_S}$$

were σ_{TPA} is the two-photon cross section and $\langle F\rangle$ the signal read by the detector, quadratically dependent on the excitation intensity. C is the concentration of the compound, η is the FQY, and ϕ is a correction factor taking into account the collection efficiency. The subscripts R and S refer to reference and sample, respectively. ϕ depends on the geometry of the experimental apparatus employed, the wavelength dependence of the filters, the refractive index of the solutions, the detector spectral response and any reabsorption effects from solution.

The optical gain properties of the QD doped sol−gel matrices were characterized through ASE measurements. These were performed at room temperature using a Ti:Sapphire amplified laser system (Spectra Physics), with pulses of 150 fs, 1 kHz repetition rate and 0.7 mJ energy at 800 nm. The intensity of the input beam was varied with neutral density filters and, for fine-tuning, with a half waveplate in series with a polarizer. The beam was focused with a 20 cm focal length cylindrical lens onto the sample. The edge emitted beam, in a lateral configuration, was detected by an optical fiber connected to a microspectrometer (Ocean Optics HR2000).

3. RESULTS AND DISCUSSION

3.1. Optical Characterization in Solution. In Figure 1, we show the linear absorption and emission characteristics of all the

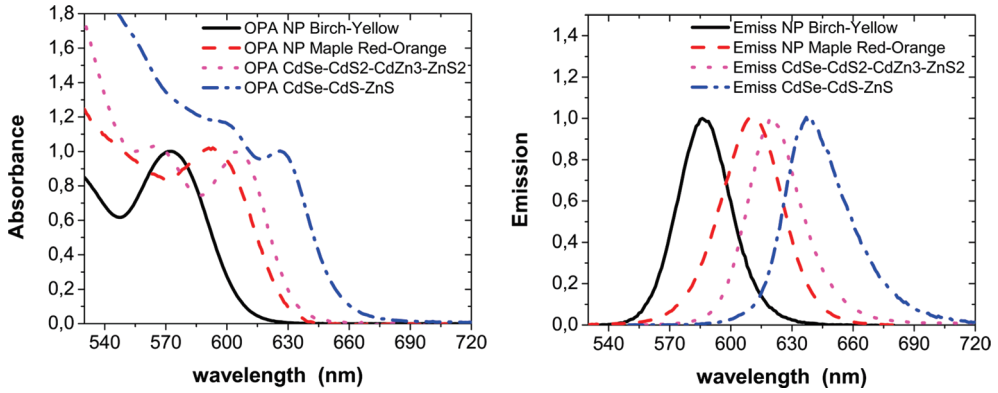

Figure 1. Linear absorption and emission spectra of commercial NP (birch−yellow and maple red−orange) in toluene and of in-house synthesized core−shell QDs (CdSe−CdS2−CdZn3−ZnS2 in isopropanol and CdSe−CdS−ZnS in ethanol).

Table 1. Linear and Nonlinear Optical Characteristics of the Different Core-Shell QDs Used in This Study

sample	QDs diameter [nm]	1st excitonic peak [nm]	emission peak [nm]	band-edge molar extinction [cm^{-1} M^{-1}]	σ_{TPA} @ 800 nm [GM]
NP birch−yellow	4.6	572	587	1.35×10^5	4000 ± 500
NP maple red−orange	5.5	593	612	2.65×10^5	16 000 ± 2000
CdSe−CdS2−CdZn3−ZnS2	8.5	606	620	2.49×10^5	21 000 ± 4200
CdSe−CdS−ZnS	7.7	626	638	4.70×10^5	45 000 ± 5000

core−shell samples studied in solution. The band-edge absorption and emission transitions of these samples fall within the orange to red spectral region. Naturally, the position of the absorption and emission peaks is directly related to the core size of QDs, but for core−shell it is additionally related to the extent of wave function leakage into the shell.[39] For this reason, differences in shell composition between our samples prevent the band-edge excitonic peaks and the emission maxima to be simply correlated to size difference alone. This is exemplified in Table 1 where we summarize the linear absorption and emission properties of samples studied here, as well as final nanocrystal diameters. A comparison between values of the band-edge molar extinction coefficient is more useful since they are less sensitive to the shell thickness for core−shells of type-I heterostructure.

The first absorption peak molar extinction coefficients of the in-house synthesized QDs were determined directly from known extinction coefficients of the core nanocrystals.[40] By assuming no dissolution of the nanocrystals during the shell deposition, a corrected band-edge molar extinction value could be determined for the core−shell QDs. The molar extinction coefficient values of commercial nanocrystals, were obtained directly from data reported in the specification sheet.[41]

To effectively extend the linear QD absorption characteristics to the nonlinear optical range, the TPIF technique can be used, provided that the samples possess high fluorescence quantum yields and the nanoparticle concentrations are accurately known. The measured FQY of the QDs, studied here, was 0.60 ± 0.03, 0.67 ± 0.03, 0.29 ± 0.01, and 0.17 ± 0.005 for birch−yellow, maple red−orange, CdSe−CdS2−CdZn3−ZnS2, and CdSe−CdS−ZnS, respectively. These values are sufficiently high for TPIF. Nanoparticle concentrations were determined based on the extinction coefficient evaluated above.

Figure 2 reports the TPA response of commercial nanocrystals and in-house synthesized core−shell QDs. For ease of comparison with the one-photon absorption (OPA) spectra, the wavelength of TPA data has been halved. The errors in the TPA cross sections are calculated from the propagation error formula, taking into account the uncertainties on sample and reference concentrations and FQY values. The error on the TPA cross sections of the standards, derived from the literature (about 30%), has not been considered.[42] Additionally, absolute values of σ_{TPA} for commercial QDs may possess inherently large errors due to uncertainties of tabulated molar extinction coefficients.

To make a quantitative comparison between samples, we consider the TPA response at 800 nm (summarized in Table 1) and the dependence of the σ_{TPA} with the QD volume (reported in Figure 3). The TPA cross-section increases with nanocrystal dimensions, with the exception of CdSe−CdS2−CdZn3−ZnS2 quantum dots. This core−shell sample varied from the other samples in that its shell composition contained an increased CdS component compared to the ZnS. CdS has been shown to act like an optical antenna for CdSe-based cores, hence providing greater absorption at wavelengths below ∼500 nm.[43] Therefore, whereas the band-edge molar exctinction coefficient still reflects the core-size (diameter ∼3.5 nm), we believe that the CdS is influencing the TPA efficiency when the excitation falls within the semicontinuum region.

The fitting of the $\log(\sigma_{TPA})$ versus $\log(Vol_{QD})$ data, as shown in Figure 3, has been performed by considering (a) all four samples and (b) by excluding the CdSe−CdS2−CdZn3−ZnS2 sample (the value depicted by the dotted circle) from the data set. In case (a), the linear curve fit gives a slope of 0.98 (black line), however the R^2 value (0.54) of this fit is unacceptably high. The slope in case (b) is 1.50 (red line), with a significant improvement to the R^2 value (0.87). Considering (b) as the more meaningful comparison based on the above reasoning, it suggests that the TPA cross sections at 800 nm of the core−shell QDs studied increase with particle dimensions as $\sigma_{TPA} \propto R^{4.5}$.

Theoretical calculations indicate that QDs TPA cross-section should scale with particle size as $\sigma_{TPA} \propto R^n$, with n being between 3 and 6, depending on the involved two-photon absorption mechanism.[44] Experimental studies performed on CdSe and CdTe cores have confirmed these predictions, with TPA cross sections scaling as $R^{3.5}$ and $R^{5.6}$, respectively.[44,45] Our results are

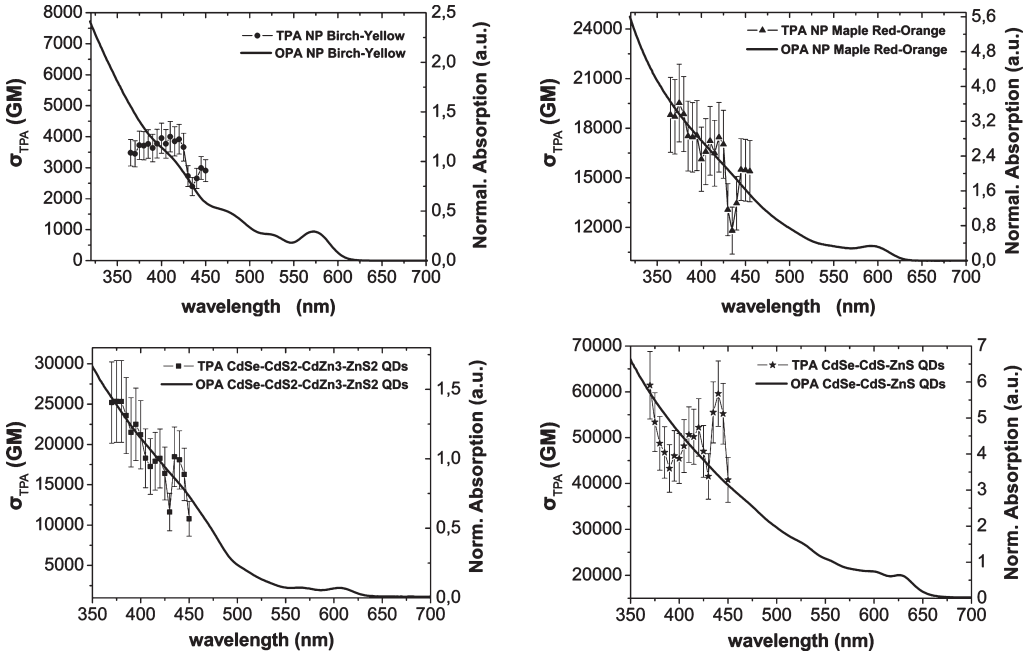

Figure 2. TPA and OPA spectra of commercial NP (upper panels) and of synthesized core−shell QDs (lower panels).

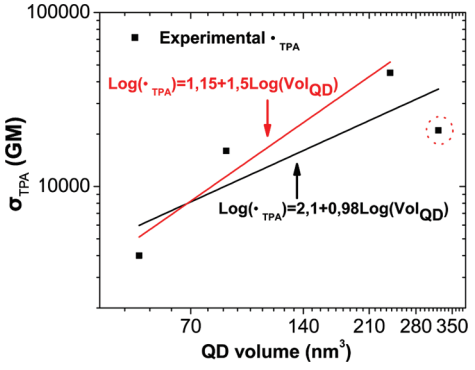

Figure 3. Log plot of experimental TPA cross-section values versus QD volume. Black and red lines are linear fitting curves considering all sample data and masking CdSe−CdS2−CdZn3−ZnS2 (value in the dotted circle), respectively.

in good agreement with these previously evidenced trends for the nonlinear optical efficiency of the TPA process.

3.2. Use of CdSe-Based Core−Shell Nanocrystals for Up-Conversion Applications. Large TPA cross sections and good emission properties make QDs a viable materials for up-converted emission based applications. To effectively exploit their lucrative properties, it is imperative that appropriate QD doped solid-state materials are firstly developed. Such materials require that (i) the surface chemistry of the QDs is appropriate to ensure homogeneous dispersion within the host and (ii) that the host matrix does not aid in the physical or photophysical long-term degradation of the QDs. Our previous efforts have shown that zirconia based sol−gel matrices are good hosts for CdSe-based QDs.[30] To prepare such hybrid materials, the original hydrophobic ligands surrounding the QD surface are exchanged with either 1-aminopentanol or 1-aminohexanol to allow for solubilization in isopropanol or ethanol.[14] This surface exchange permits for homogeneous dispersion of the core−shell QDs compatible within the sol−gel matrix. Within this study, such a procedure could only be made successfully with the in-house prepared QDs, whose known surface chemistry permitted for a well controlled ligand exchange. Following ligand exchange, here we used the in-house synthesized and alcohol soluble QDs as dopants within two electronically similar sol−gel matrices: hafnia and zirconia. Our previously successful employment of using zirconia as a host matrix for CdSe QDs stemmed from the type-I electronic configuration that it form with respect to the CdSe QDs (part a of Figure 4). The energy diagram based on literature values of the core, shell and host matrix components utilized in this study is illustrated in part b of Figure 4 (ZnS, ZrO_2,[47] CdSe,[48] HfO_2[49]) . The condition of a type-I configuration for cores with respect to the shell and both HfO_2 and ZrO_2 matrices are clearly met.

For the characterization of the up-conversion process, ASE measurements of QDs doped ZrO_2 and HfO_2 hybrid matrices were performed under two-photon excitation (at 800 nm) in a lateral configuration.[14] The typical emission behavior for both composites are depicted in Figure 5, and further summarized in Table 2. At low excitation power only the spontaneous emission is detected; increasing the fluence above the optical gain threshold, results in a red-shifted and spectrally narrower (FWHM ∼10 nm) ASE counterpart. The nearly identical ASE threshold fluences for the same QDs in both matrices is a reflection of their comparable electronic properties.

The ASE peak for both quantum dots is red-shifted with respect to the maximum of the spontaneous emission band in solution by ∼16 meV and ∼40 meV for the CdSe−CdS2−CdZn3−ZnS2 and CdSe−CdS−ZnS QD samples, respectively. This energy loss, with respect to the single exciton emission, has been correlated to the stabilization energy of the biexcitonic state.[17] For CdSe based type-I core−shell QDs, typical stabilization energies are between 30 and 40 meV. The measured data of CdSe−CdS−ZnS QDs falls within this range. In contrast, the CdSe−CdS2−CdZn3−ZnS2 sample exhibits a much lower value. At present, we do not completely understand why such lower stabilization energy is observed for this sample. Recent

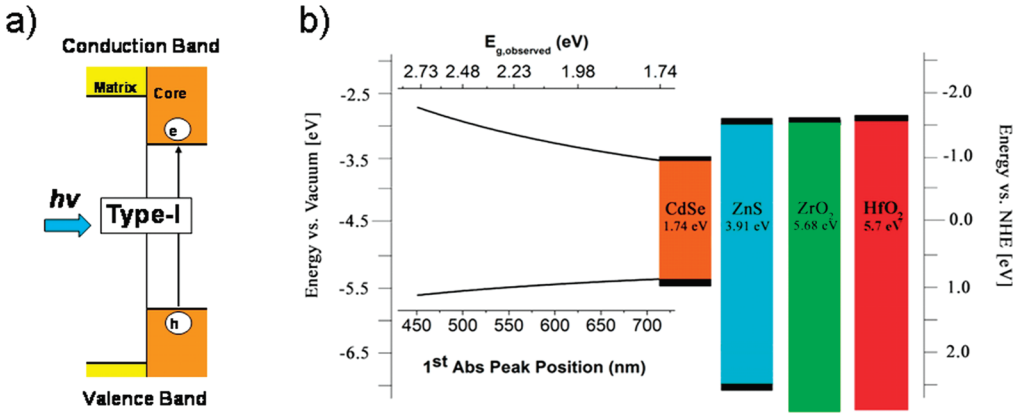

Figure 4. Localization of the electron and hole carriers across a heterostructure interface in a type-I configuration (a); scheme of the electron affinities, ionization potentials and band gap energies of CdSe (as a function of the first exciton peak), ZnS and ZrO_2 and HfO_2 (b).

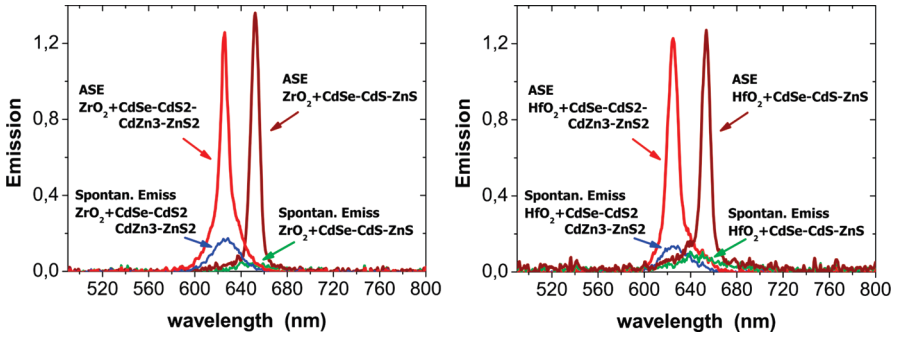

Figure 5. Spontaneous and amplified spontaneous emission signals for ZrO_2−QDs (left panel) and HfO_2−QDs (right panel) waveguides under two-photon excitation at 800 nm.

Table 2. ASE Emission Features of QD-Doped ZrO_2 and HfO_2 Thin-Films under 800 nm Two-Photon Optical Pumping

sample	ASE peak [nm]	FWHM [nm]	fluence threshold [mJ/cm^2]
ZrO_2 + CdSe−CdS2−CdZn3−ZnS2	625.8	9	6.8
HfO_2 + CdSe−CdS2−CdZn3−ZnS2	625.0	11	5.9
ZrO_2 + CdSe−CdS−ZnS	652.0	7	8.1
HfO_2 + CdSe−CdS−ZnS	653.5	9.5	7.3

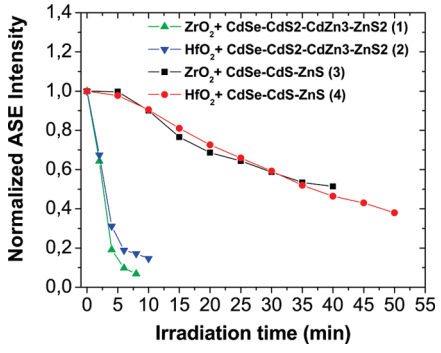

Figure 6. Temporal stability of two-photon induced ASE stability of the hybrid QD doped sol−gel waveguides. The fluences for these samples were 17.3 mJ/cm^2 for composites 1−3 and 10.2 mJ/cm^2 for composite 4.

studies hint that this observation may be related to variations in shell-assisted interfacial or surface trap passivation and/or differences in the multiexcitonic states, populated by the optical pump and then probed during the ASE measurement.[28,50] Inherently, the nature of these states must reflect the composition of the shell material and the method by which it was deposited. Studies are under way to further understand these influences more clearly.

3.3. Photostability under Prolonged Irradiation. The development of ASE with similar thresholds in both hafnia and zirconia matrices infers that the optical gain properties of the QDs are comparable in both hosts. To further explore how these hosts compare, in Figure 6 we show the ASE intensity as a function of the irradiation time. Under continuous optical pumping, with similar fluences, the intensity of the ASE peak for CdSe−CdS2−CdZn3−ZnS2 QD composites decreases rapidly in the first 5 min in both HfO_2 and ZrO_2 matrices. In contrast, the ASE for the CdSe−CdS−ZnS films is stable for the initial 10 min, and gradually decreases to 50% of its initial intensity after ∼40 min irradiation. Again, this behavior is the same for zirconia and hafnia matrices. The similarity of the QD photophysical behavior in these hosts must reflect their nearly identical optical properties, such as band gap, electron affinities and ionization potentials. This observation establishes that high

band gap, low electron affinity, and high ionization potential sol−gel metal oxides are suitable hosts for CdSe and presumably many other compositions, based QDs.

The cause of the large difference in the photostability between our samples, obtained from two different syntheses and possessing different final shell structures, is not completely clear. It has been reported that thicker shells cause increasing interfacial strain between the core and the shell.[39] This results in larger defect formation at this interface, which would undoubtedly also increase the number of deactivation pathways in competition with the amplified spontaneous emission process. Moreover, the stronger residual absorption due to the thicker shell, in the semicontinuum region, could also affect the photostability of CdSe−CdS2−CdZn3−ZnS2 sample. While further studies regarding this issue are under way, this result does definitively highlight that high photostability of QDs is not correlated to quantum yield, which is higher for the less stable CdSe−CdS2−CdZn3−ZnS2 QDs.

4. CONCLUSIONS

The linear and nonlinear optical properties of commercial and in-house synthesized core−shell quantum dots have been studied. The measured size-dependent TPA efficiencies are in good agreement with previous studies, reaching a maximum value of 45 000 GM for red emitting 7.7 nm CdSe−CdS−ZnS QDs. Following appropriate surface functionalization, QDs with different structures and emission wavelengths were embedded into sol−gel zirconia and hafnia host matrices. Up-converted amplified spontaneous emission in both hybrid matrices was demonstrated. Owing to the similar electronic properties of the sol−gel hosts, comparable behavior was observed for all QD types. These results highlight the importance of choosing an appropriate host and ensuring that the highest quality core−shell nanocrystals are used for the development of QD-based hybrid materials useful in future photonic applications.

AUTHOR INFORMATION

Corresponding Author

*Fax: +39 049 8275239, phone: +39 049 8275118, e-mail: raffaella.signorini@unipd.it.

ACKNOWLEDGMENT

We acknowledge funding from the PRIN 2007 (2007LN873M_001) grant from the Italian Ministry of Education and Research (MiUR) and from the PROMO CNR-INSTM contract. Prof. G. Guglielmi thanks the EU commission for financial support trough 6FP “MULTIPRO” project.

REFERENCES

(1) Boyd, R. W. *Nonlinear Optics*; Academic Press Elsevier Science (USA): New York, 1992.
(2) *Femtochemistry*; Wiley-VCH: Germany: Weiheim, 2001.
(3) Lee, H. W.; Kim, Y. M.; Jeon, D. J.; Kim, E.; Kim, J.; Park, K. *Opt. Mater.* **2003**, *21*, 289.
(4) Devaraj, B.; Usa, M.; Chan, K. P.; Akatsuka, T.; Inaba, H. *IEEE J. Quantum Electron.* **1996**, *2*, 1008.
(5) Leveque-Fort, S.; Papadopoulos, D. N.; Forget, S.; Balembois, F.; Georges, P. *Opt. Lett.* **2005**, *30*, 168.
(6) Ponce, F. A.; Bour, D. P. *Nature* **1997**, *386*, 351.
(7) Abbotto, A.; Beverina, L.; Bozio, R.; Bradamante, S.; Ferrante, C.; Pagani, G. A.; Signorini, R. *Adv. Mater.* **2000**, *12*, 1963.
(8) Scheps, R. *Prog. Quantum Electron.* **1996**, *20*, 271.
(9) He, G. S.; Zhao, C. F.; Bhawalkar, J. D.; Prasad, P. N. *Appl. Phys. Lett.* **1995**, *67*, 3703.
(10) He, G. S.; Signorini, R.; Prasad, P. N. *IEEE J. Quantum Electron.* **1998**, *34*, 7.
(11) Zhang, H. C.; Guo, E. Q.; Zhang, X. H.; Yang, W. J. *J. Polym. Sci., Part A: Polym. Chem.* **2010**, *48*, 463.
(12) Xie, R. G.; Kolb, U.; Li, J. X.; Basche, T.; Mews, A. *J. Am. Chem. Soc.* **2005**, *127*, 7480.
(13) Larson, D. R.; Zipfel, W. R.; Williams, R. M.; Clark, S. W.; Bruchez, M. P.; Wise, F. W.; Webb, W. W. *Science* **2003**, *300*, 1434.
(14) Jasieniak, J. J.; Fortunati, I.; Gardin, S.; Signorini, R.; Bozio, R.; Martucci, A.; Mulvaney, P. *Adv. Mater.* **2008**, *20*, 69.
(15) Zhang, C. F.; Zhang, F.; Cheng, A.; Kimball, B.; Wang, A. Y.; Xu, J. *Appl. Phys. Lett.* **2009**, 95.
(16) Alivisatos, A. P. *Science* **1996**, *271*, 933.
(17) Klimov, V.; Hunsche, S.; Kurz, H. *Phys. Rev. B* **1994**, *50*, 8110.
(18) Shim, M.; Guyot-Sionnest, P. *Nature* **2000**, *407*, 981.
(19) Piryatinski, A.; Ivanov, S. A.; Tretiak, S.; Klimov, V. I. *Nano Lett.* **2007**, *7*, 108.
(20) Achermann, M.; Petruska, M. A.; Koleske, D. D.; Crawford, M. H.; Klimov, V. I. *Nano Lett.* **2006**, *6*, 1396.
(21) Schaller, R. D.; Agranovich, V. M.; Klimov, V. I. *Nature Physics* **2005**, *1*, 189.
(22) Ravindran, S.; Ozkan, C. S. *Nanotechnology* **2005**, *16*, 1130.
(23) Medintz, I. L.; Uyeda, H. T.; Goldman, E. R.; Mattoussi, H. *Nat. Mater.* **2005**, *4*, 435.
(24) Stroh, M.; Zimmer, J. P.; Duda, D. G.; Levchenko, T. S.; Cohen, K. S.; Brown, E. B.; Scadden, D. T.; Torchilin, V. P.; Bawendi, M. G.; Fukumura, D.; Jain, R. K. *Nature Medicine* **2005**, *11*, 678.
(25) Grecco, H. E.; Lidke, K. A.; Heintzmann, R.; Lidke, D. S.; Spagnuolo, C.; Martinez, O. E.; Jares-Erijman, E. A.; Jovin, T. M. *Microscopy Research and Technique* **2004**, *65*, 169.
(26) Rizzo, A.; Li, Y. Q.; Kudera, S.; Della Sala, F.; Zanella, M.; Parak, W. J.; Cingolani, R.; Manna, L.; Gigli, G. *Appl. Phys. Lett.* **2007**, 90.
(27) Malko, A. V.; Mikhailovsky, A. A.; Petruska, M. A.; Hollingsworth, J. A.; Htoon, H.; Bawendi, M. G.; Klimov, V. I. *Appl. Phys. Lett.* **2002**, *81*, 1303.
(28) Cooney, R. R.; Sewall, S. L.; Sagar, D. M.; Kambhampati, P. *Phys. Rev. Lett.* **2009**, 102.
(29) Klimov, V. I.; Ivanov, S. A.; Nanda, J.; Achermann, M.; Bezel, I.; McGuire, J. A.; Piryatinski, A. *Nature* **2007**, *447*, 441.
(30) Jasieniak, J.; Pacifico, J.; Signorini, R.; Chiasera, A.; Ferrari, M.; Martucci, A.; Mulvaney, P. *Adv. Funct. Mater.* **2007**, *17*, 1654.
(31) Li, J. J.; Wang, Y. A.; Guo, W. Z.; Keay, J. C.; Mishima, T. D.; Johnson, M. B.; Peng, X. G. *J. Am. Chem. Soc.* **2003**, *125*, 12567.
(32) van Embden, J.; Mulvaney, P. *Langmuir* **2005**, *21*, 10226.
(33) van Embden, J.; Jasieniak, J.; Gomez, D. E.; Mulvaney, P.; Giersig, M. *Aust. J. Chem.* **2007**, *60*, 457.
(34) Jasieniak, J.; Mulvaney, P. *J. Am. Chem. Soc.* **2007**, *129*, 2841.
(35) Bindhu, C. V.; Harilal, S. S.; Varier, G. K.; Issac, R. C.; Nampoori, V. P. N.; Vallabhan, C. P. G. *J. Phys. D: Appl. Phys.* **1996**, *29*, 1074.
(36) Isak, S. J.; Eyring, E. M. *J. Phys. Chem.* **1992**, *96*, 1738.
(37) Demas, J. N.; Crosby, G. A. *J. Phys. Chem.* **1971**, *78*, 991.
(38) Rumi, M.; Ehrlich, J. E.; Heikal, A. A.; Perry, J. W.; Barlow, S.; Hu, Z. Y.; McCord-Maughon, D.; Parker, T. C.; Rockel, H.; Thayumanavan, S.; Marder, S. R.; Beljonne, D.; Bredas, J. L. *J. Am. Chem. Soc.* **2000**, *122*, 9500.
(39) Dabbousi, B. O.; RodriguezViejo, J.; Mikulec, F. V.; Heine, J. R.; Mattoussi, H.; Ober, R.; Jensen, K. F.; Bawendi, M. G. *J. Phys. Chem. B* **1997**, *101*, 9463.
(40) Jasieniak, J.; Smith, L.; van Embden, J.; Mulvaney, P.; Califano, M. *J. Phys. Chem. C* **2009**, *113*, 19468.
(41) The measured absorption peaks in solution for these commercial QDs were not coincident with those reported in the specification

sheet. For this reason, final molar extinction coefficients had to be extrapolated from the complete EviDot series calibration curve. This method of approximating the molar extinction coefficient suggests a possible source of error in the determination of the final concentration of these nanocrystals.

(42) Xu, C.; Williams, R. M.; Zipfel, W.; Webb, W. W. *Bioimaging* **1996**, *4*, 198.
(43) Talapin, D. V.; Nelson, J. H.; Shevchenko, E. V.; Aloni, S.; Sadtler, B.; Alivisatos, A. P. *Nano Lett.* **2007**, *7*, 2951.
(44) Pu, S. C.; Yang, M. J.; Hsu, C. C.; Lai, C. W.; Hsieh, C. C.; Lin, S. H.; Cheng, Y. M.; Chou, P. T. *Small* **2006**, *2*, 1308.
(45) Klimov, V. I. *J. Phys. Chem. B* **2000**, *104*, 6112.
(46) He, G. S.; Yong, K. T.; Zheng, Q. D.; Sahoo, Y.; Baev, A.; Ryasnyanskiy, A. I.; Prasad, P. N. *Optics Express* **2007**, *15*, 12818.
(47) Xu, Y.; Schoonen, M. A. A. *Am. Mineral.* **2000**, *85*, 543.
(48) Kucur, E.; Riegler, J.; Urban, G. A.; Nann, T. *J. Chem. Phys.* **2003**, *119*, 2333.
(49) Balog, M.; Schleber, M.; Michman, M.; Patai, S. *Thin Solid Films* **1977**, *41*, 247.
(50) Cooney, R. R.; Sewall, S. L.; Sagar, D. M.; Kambhampati, P. *J. Chem. Phys.* **2009**, 131.